# Supplemental Materials

***Molecular Biology of the Cell***

Murata et al.

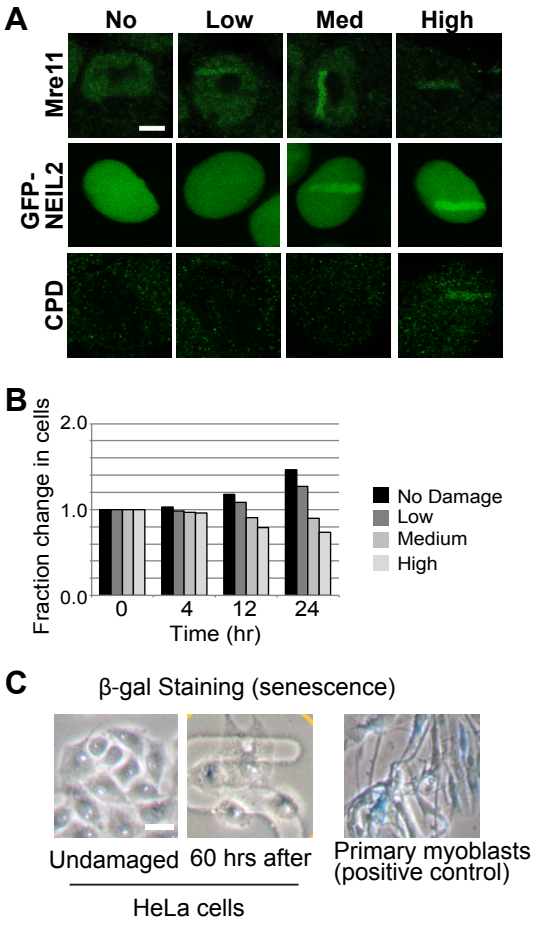


**Supplemental Figure S1. Characterization of DNA damage and cell fate following laser microirradiation using different input power.**
(A) Immuno-fluorescent staining for Mre11 (top) and CPD (bottom) in HeLa cells fixed at 1 hr post damage following low, medium, and high input laser power. Fluorescent images for HeLa cells expressing GFP-Neil2 (middle) at approximately 2 min following low, medium, and high input laser power. Scale bar = 5 μm.
(B) The fraction change in the total number of HeLa cells over time following low, medium, and high input laser power. N=50.
(C) β-galactosidase staining of undamaged HeLa cells and cells at 60 hr post laser microirradiation at high input-power. Primary myoblasts were stained as a positive control. N=15. Scale bar = 20 μm.

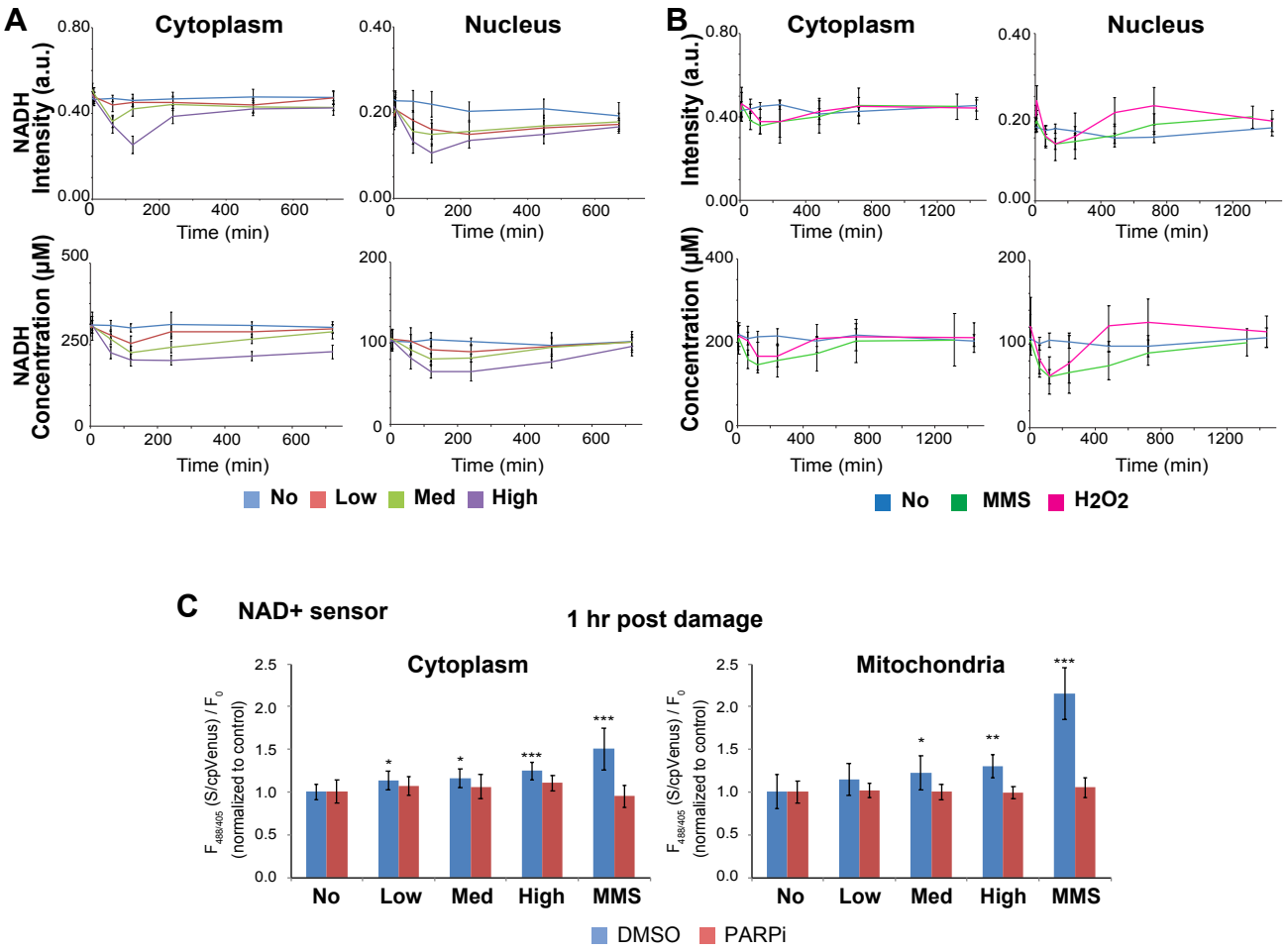


**Supplemental Figure S2. Laser Damage Induces Dose-Dependent Decrease in NADH Intensity and Concentration.**

(A) The intensity of NADH and concentration of NADH over time in the cytoplasmic and nuclear compartments of HeLa cells following low, medium, and high input laser power. N=25.

(B) The intensity of NADH and concentration of NADH over time in the cytoplasmic and nuclear compartments of HeLa cells treated with either 1 mM MMS or 500 µM H2O2. N=25.

(C) The change in the ratiometric fluorescence intensity of the cytoplasmic or mitochondrial NAD+ biosensor at 1 hr post damage following low, medium, and high laser microirradiation or 3 mM MMS treatment for 1 hr. Cells were treated with either 0.1% DMSO or 20 µM PARP inhibitor (olaparib). An increased fluorescence ratio reflects decreased NAD+ binding. N=25.

* $p < 0.05$, ** $p < 0.01$, *** $p < 0.001$.

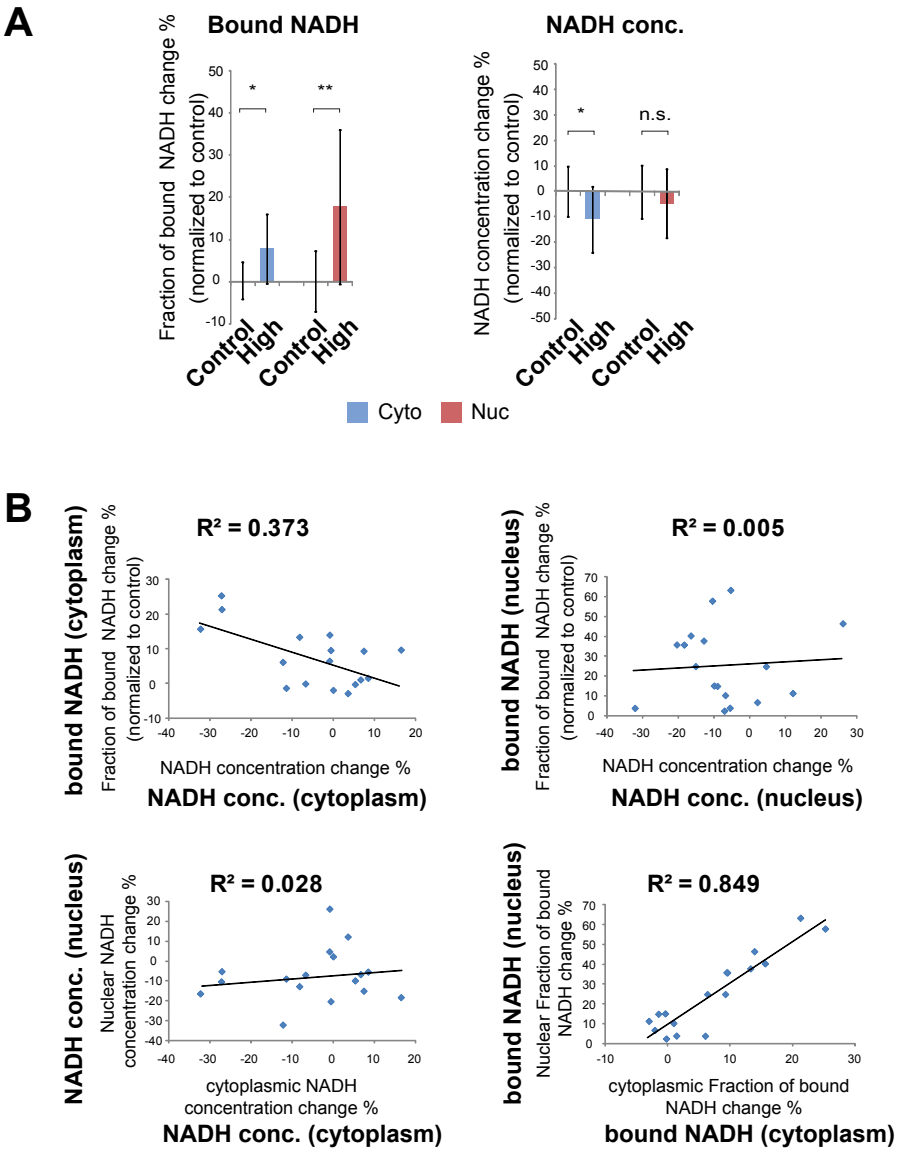


**Supplemental Figure S3. Correlation between cytoplasmic and nuclear NADH concentrations and bound NADH fractions.**

(A) At 12 hr post damage, the percent change of the fraction of bound NADH (left) and the concentration of NADH (right) in the cytoplasm and nucleus of undamaged HeLa cells (Control) or HeLa cells damaged with high input power laser microirradiation (High). The data was normalized with that of the undamaged control cells. N=15. * $p<0.05$, ** $p< 0.01$, n.s. $p>0.05$.
(B) Scatter plots examining the correlation between the percent changes of the NADH concentration and bound NADH in the cytoplasm and nucleus of the individual damaged cell from (A). The line represents the trendline, and the R-squared value was calculated in Excel and measures the strength of the relationship between data and trendline.

**Supplemental Figure S4**

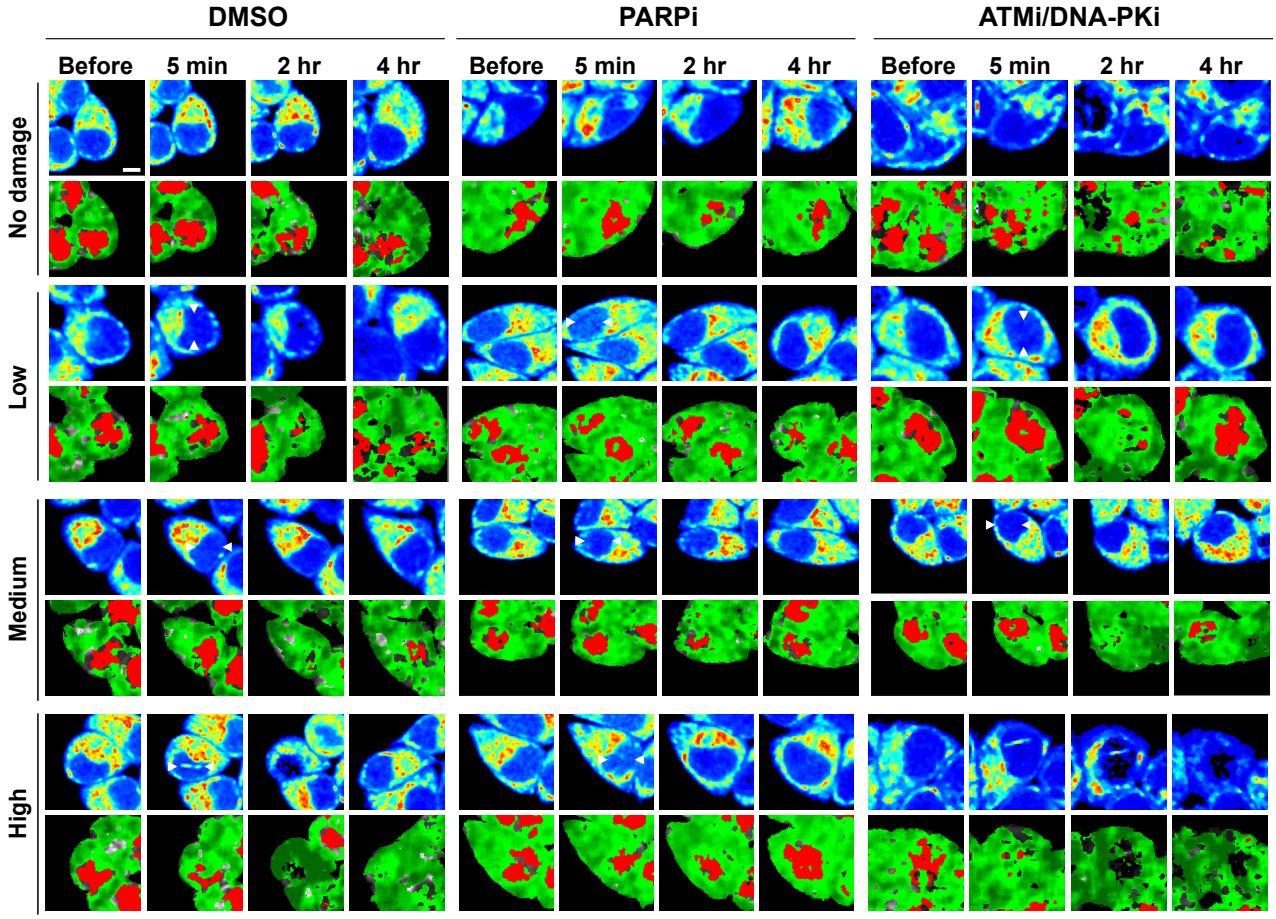


**Supplemental Figure S4. Damage-induced changes in NADH intensity and FLIM images are PARP, but not ATM/DNA-PK,-dependent.**
Intensity (top) and pseudo-colored FLIM (bottom) images of undamaged HeLa cells and HeLa cells damaged at low, medium, and high input laser power and treated with either 0.1% DMSO (left), 20 µM PARP inhibitor (olaparib) (middle), or 10 µM ATM inhibitor (KU55933) and 10 µM DNA-PK inhibitor (NU7026) (right). In intensity images, the line color from blue to red corresponds to the normalized intensity. Damage sites are indicated by white arrows.
The FLIM images are pseudo-colored according to the clusters selected on the phasor plot in (Figure 1B). Scale bar = 5 µm.

**Supplemental Figure S5**

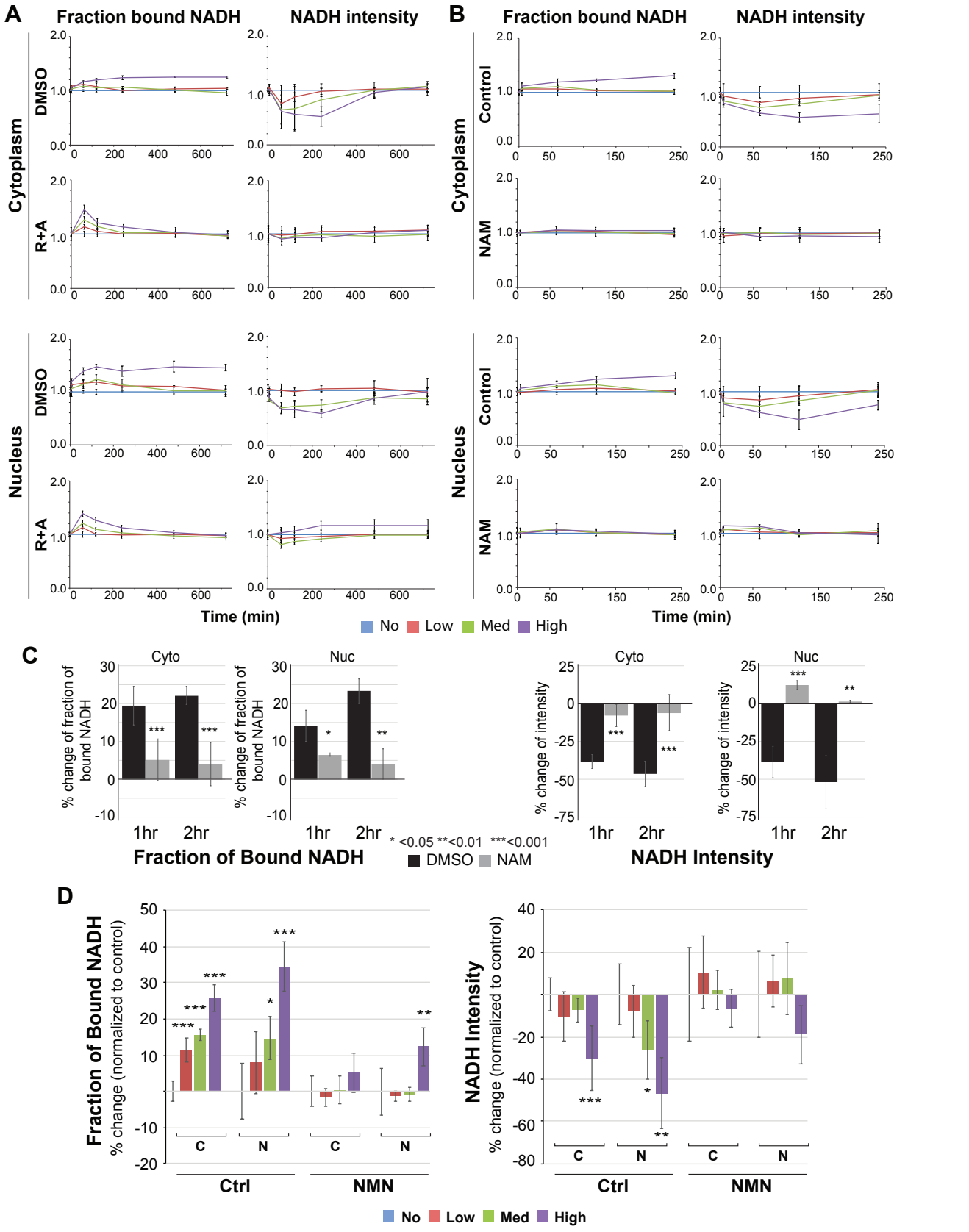

**Supplemental Figure S5. Laser damage-induced increase of bound NADH and decrease of NADH intensity are suppressed by the respiratory chain inhibitors and NAD replenishment.**

(A) The change in fraction of bound NADH (left) and intensity of NADH (right) in the cytoplasmic (top) and nuclear (bottom) compartments plotted over time in cells damaged with low, medium, and high input laser power in the presence of control (0.1% DMSO) or 1 μM rotenone and 1 μM antimycin A (R+A) as indicated. Comparison of bound NADH in the cytoplasm (Left top) is same as Figure 3A left. N=20.

(B) The change in the fraction of bound NADH (left) and intensity of NADH (right) over time in cells damaged with low, medium, and high input laser power in control cells and cells pre-treated for 1 hr with 1 mM NAM. Data was normalized to initial value before damage. N=20.

(C) The change in the fraction of bound NADH (left) and the intensity of NADH (right) at 1 hr and 2 hr post damage with 1 mM NAM relative to basal conditions. N=15. * $p < 0.05$, ** $p < 0.01$, *** $p < 0.001$.

(D) The percent change in the fraction of bound NADH (left) and the intensity of NADH (right) at 2 hr post damage with 1 mM NMN relative to basal conditions. N=10. * $p < 0.05$, ** $p < 0.01$,*** $p < 0.001$.

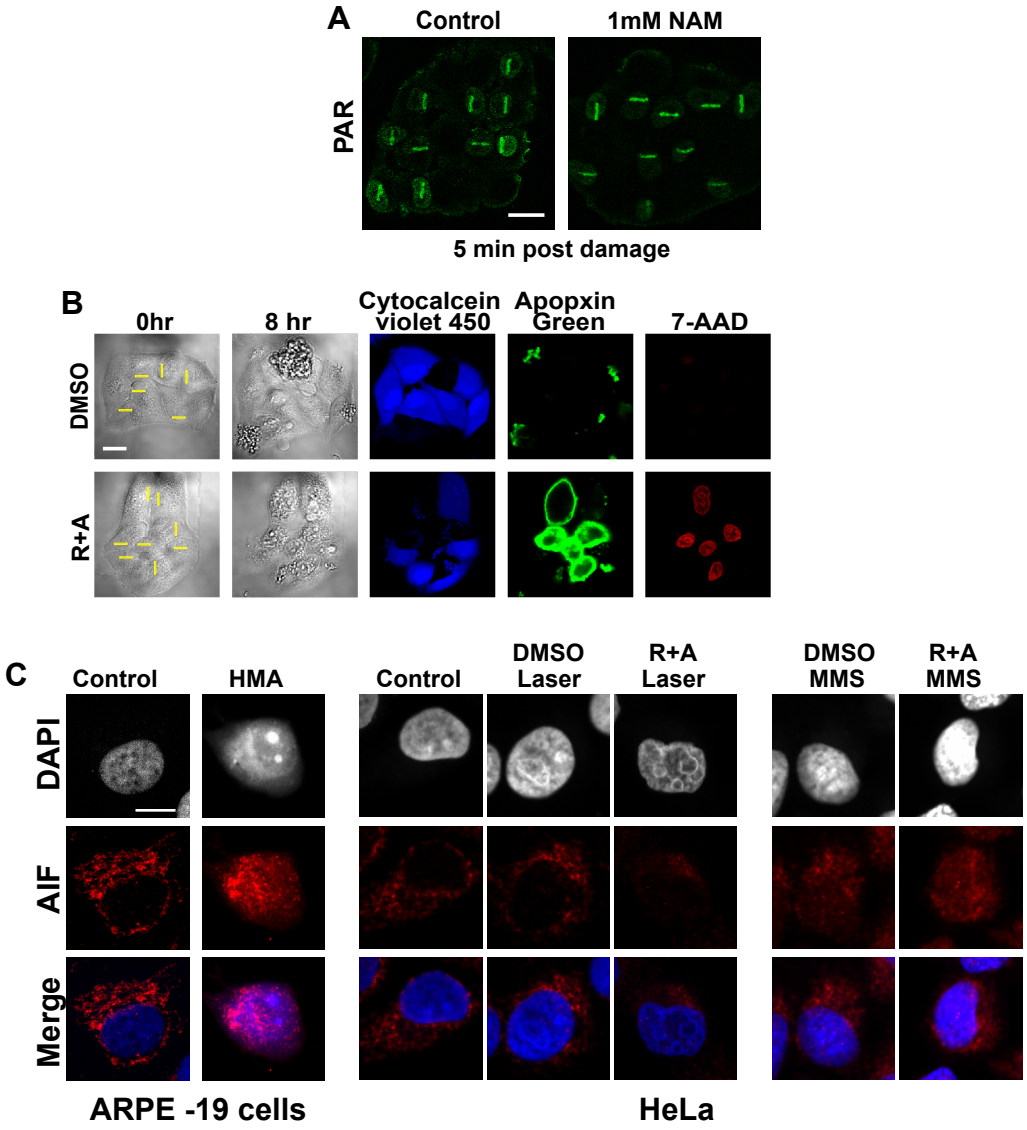


**Supplemental Figure S6. Damage-specific cell death induced by R+A treatment is AIF-independent apoptosis.**

(A) Immuno-fluorescent staining for PAR (green) in HeLa cells pre-treated with or without 1 mM NAM for 1 hr and fixed 5 min post damage following low, medium, and high input laser power. Scale bar = 20 µm.

(B) Brightfield images of HeLa cells treated with either 0.2 % DMSO or 1 µM rotenone and 1 µM antimycin A before damage and 8 hr post damage. Apoptosis and necrosis was detected using a commercial kit (AB176749) for live cells (cytocalcein violet 450, blue), phosphatidylserine exposure (apopxin green, green), and loss of plasma integrity (7-aminoactinomycin D, red). Scale bar = 20 µm.

(C) Immuno-fluorescent staining for apoptosis inducing factor (AIF) and DAPI in HeLa cells at 8 hr post damage induced by high input power laser or 3 mM MMS, with DMSO or rotenone and antimycin (R+A) treatment. As a positive control, human adult retinal pigmented epithelial (ARPE-19) cells were treated for 24 hr with 120 µM 5-(N,N-hexamethylene)amiloride (HMA) (the left panel). The ARPE-19 cells became rounded and AIF appeared to move to the nucleus in response to MMS (the right panel), but not by laser damage (the middle panel). Scale bar = 10 µm.

## Supplemental Figure S7

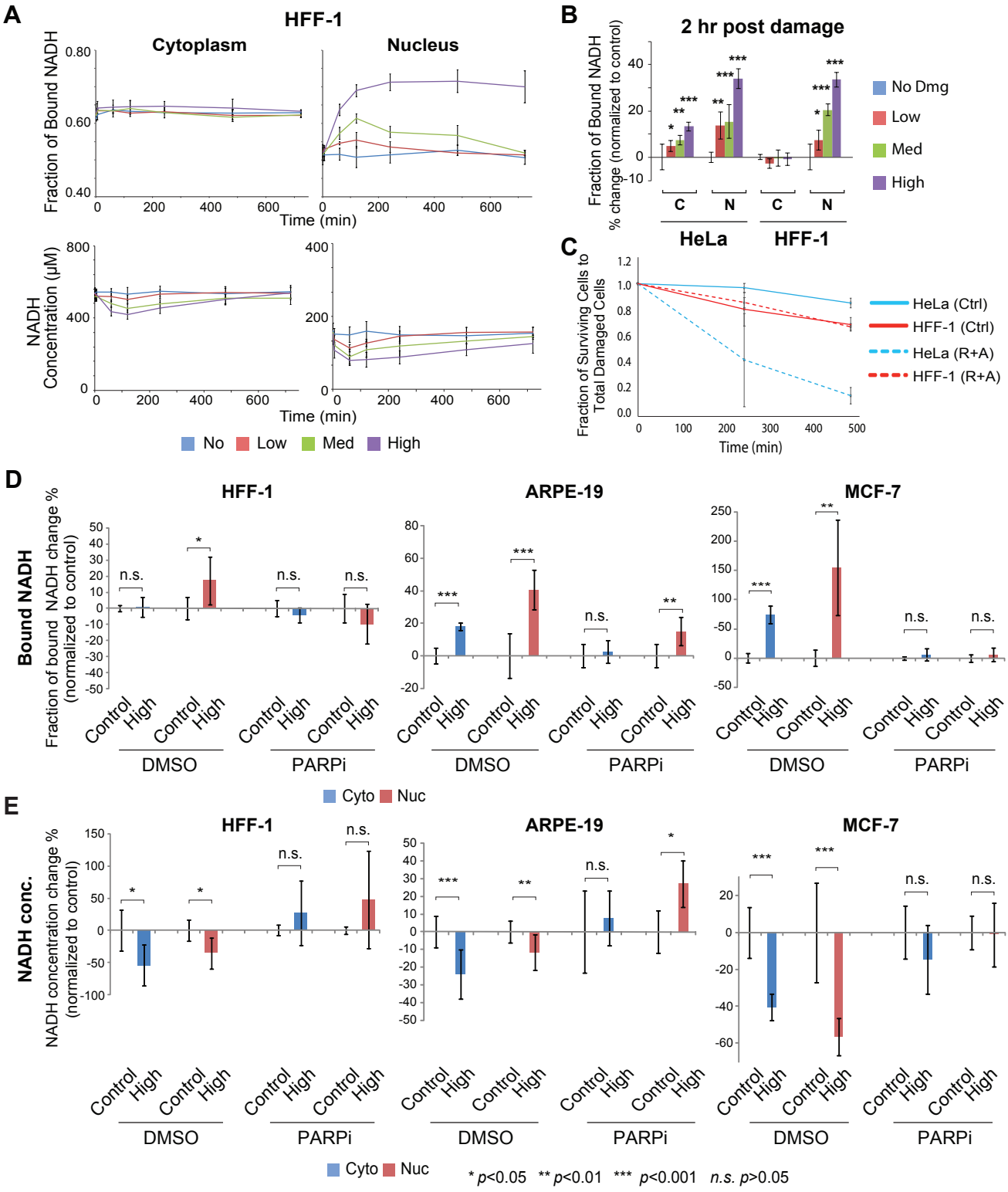

**Supplemental Figure S7. Differential free to bound NADH shift in different cell types**
(A) The fraction of bound NADH in the cytoplasmic and nuclear compartments in primary HFF-1 cells following laser damage induction. Corresponding NADH concentration measurement is shown underneath. N=15.
(B) The percent change in the fraction of bound NADH in HeLa and HFF-1 cells at 2 hr post damage relative to basal conditions. N=15. * $p < 0.05$, ** $p < 0.01$, *** $p < 0.001$.
(C) Differential sensitivity of HeLa and HFF-1 to oxphos inhibition in laser-damaged cells. Following high input power damage, HFF-1 cells failed to show any increase in sensitivity to respiratory inhibition. N=50.
(D) Phasor-FLIM analysis of PARPi sensitivity of bound NADH increase in HFF-1, ARPE-19, MCF7 cells in response to high power laser induced damage. N=10 * $p < 0.05$, ** $p < 0.01$, *** $p < 0.001$, n.s. $p>0.05$.
(E) Phasor-FLIM analysis of NADH concentration changes in the same cells as in (D) in response to high power laser induced damage with DMSO or PARPi. * $p < 0.05$, ** $p < 0.01$, *** $p < 0.001$, n.s. $p>0.05$.

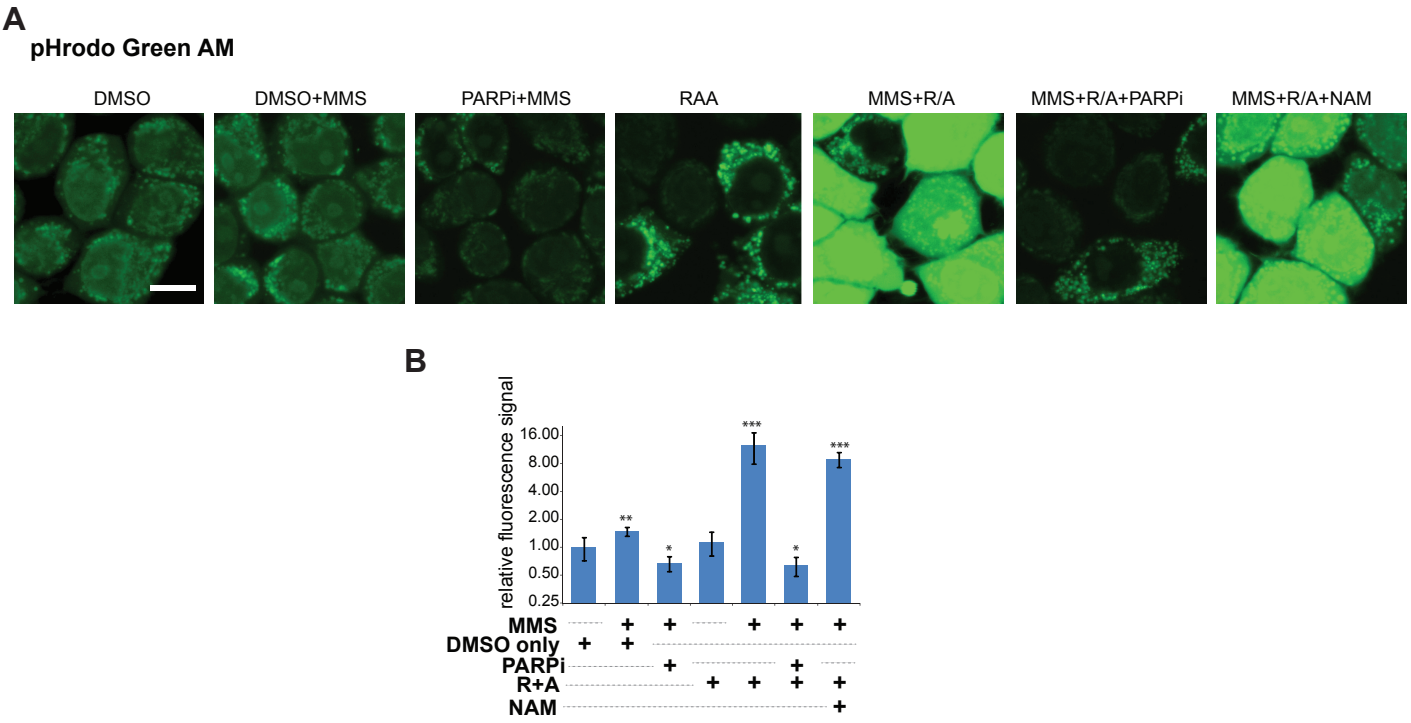


**Supplemental Figure S8. Intracellular pH (pHi) measurement using pHrodo Green AM reveal significant damage-specific acidification by R+A, which is alleviated by PARPi but not by NAM.**

(A) Fluorescence images of HeLa cells HeLa cells that were treated with indicated chemicals with or without MMS damage induction for 1 hr. After 2 hr, pHrodo Green AM was then added for 30 min and fluorescence intensities were measured by confocal microscopy. Scale bar = 10 µm. (B) Relative fluorescence intensities were quantified where higher intensities correspond to lower pH. The pHi changes were compared to cells treated with DMSO only. N=25.
* $p < 0.01$, ** $p < 0.001$, *** $p < 0.000001$.